Zero-background small-molecule sensors for near-IR fluorescent imaging of biomacromolecular targets in cells

Myar Mohamed, Anastasia K. Klenke, Maksim V. Anokhin, Harouna Amadou, Paige J. Bothwell, Brigid Conroy, Evgueni E. Nesterov,* and Irina V. Nesterova*

 $Department \ of \ Chemistry \ and \ Biochemistry, \ Northern \ Illinois \ University, \ DeKalb, \ IL \ 60115, USA. \ Corresponding \ author \ e-mail: \\ een@niu.edu; inesterova@niu.edu$

KEYWORDS Fluorescent imaging, live-cell imaging, near-IR fluorescence, phthalocyanines, H-aggregates, EGFR tyrosine kinase

ABSTRACT: In this study, we report a general approach to the design of a new generation of small-molecule sensors that produce a zero background but are brightly fluorescent in the near-IR spectral range upon selective interaction with a biomolecular target. We developed a fluorescence turn-on/off mechanism based on the aggregation/de-aggregation of phthalocyanine chromophores. As a proof-of-concept, we designed, prepared, and characterized sensors for in-cell visualization of epidermal growth factor receptor (EGFR) tyrosine kinase. We established structure/bioavailability correlation, conditions for the optimal sensor uptake and imaging, demonstrated binding specificity and applications over a wide range of treatment options involving live and fixed cells. The new approach enables high contrast imaging and require no in-cell chemical assembly or post-exposure manipulations (i.e. washes). The general design principles demonstrated in this work can be extended towards sensors and imaging agents for other biomolecular targets.

Fluorescent imaging is a powerful tool for visualization of micro- and nanoscale targets and their dynamics within *in vitro*, cellular, and/or *in vivo* setups.^{1,2} The approach is instrumental for assessing distribution, expression levels, activity, interactions, and dynamics of biomarkers ranging from ions to proteins to cell organelles in native, manipulated, and/or artificial environments.³⁻¹⁵ Small-molecule sensors play a major role in fluorescent imaging.¹⁶ Unlike their larger-size counterparts (e.g. fluorescent proteins, nanoparticles, fluorescent antibodies), small-molecule sensors do not need to be expressed endogenously, are less likely to be toxic and/or to interfere with biological functions, are compatible with living systems (in contrast to antibody-based sensors), yield high labelling density,¹⁷ and are essential for super-resolution imaging.^{17, 18} Therefore, the demand for bright and selective small-molecule fluorescent sensors remains high.

Two fundamental parameters define the value of a fluorescent sensor: target recognition characteristics (i.e. specificity and affinity) and signal transduction quality (i.e. signal-to-background change upon recognition event, brightness, and chemical/photochemical stability).^{1,4}

An effective strategy for enabling biomacromolecular target recognition involves incorporating inhibitor structures^{1, 12, 14, 15, 17, 19} or other known/derived specific binders^{6, 7, 16, 20} into a sensor's scaffold. Since inhibitor molecules are deliberately refined to bind respective targets with high affinity and selectivity, one expects the derived sensors to retain those desirable characteristics.

To enable high-quality signal generation, fluorescent probes must be sufficiently bright in their target-bound state (i.e. possess both high extinction coefficient and high fluorescent quantum yield), turn on emission upon target recognition, and preferably absorb/emit in the

far-red/near-IR spectral range (to achieve better signal-to-back-ground (S/B) ratios due to the low auto-fluorescence of biological matter beyond 600 nm). ²¹⁻²⁶ The common strategies for engineering turn-on emissive probes include masking a fluorophore followed by restoring emission upon reacting with a biomarker, ³ use of bioorthogonal chemistry to activate emission upon a sensor's interaction with a target, ^{1, 5-7, 12, 19, 27} utilizing environmentally sensitive probes (e.g. based on solvatochromism ^{15, 28, 29}), photoswitching, ⁴ and elaborating on emission changes in the chromophore aggregated/de-aggregated states. ^{30, 31} Very few of the aforementioned platforms offer a near-IR imaging capability while simultaneously providing high target recognition selectivity.

Despite various signal transduction strategies available, the majority of reported cellular imaging protocols must rely on using multiple sequentially added reagents and sensor assembly reactions inside the cells (as often required for bioorthogonal chemistry methods), or intricate multi-step washes to remove unbound sensor as a source of an excessive emissive background. The extensive manipulations or chemical functionalization of the target may conceal or alter natural processes in living systems. Such platforms are also less suitable for the developing of rapid and reliable cell-based fluorescent assays as required, for example, for high throughput screening of anticancer drug candidates. The need to minimize manipulations within native/living environments motivates the current search for new signal turn-on principles and more advanced small-molecule fluorescent sensors that do not require washes or elaborate manipulations prior to imaging.

Recently, we have developed a new paradigm for biorecognition-induced fluorescent emission activation, which is based on changes in the aggregation state of phthalocyanine (Pc) upon its binding to a

biomolecular target. $^{34-37}$ Phthalocyanines are large planar π -conjugated molecules; the intermolecular interactions between their hydrophobic aromatic cores cause Pcs to aggregate in aqueous environments (e.g. Pc dimerization constants as high as 109 have been measured).³⁸ When non-aggregated, Pcs are brightly fluorescent in the near-IR range: reported extinction coefficients are as high as 300,000 M⁻¹cm⁻¹ (e.g. ref. ³⁹) and fluorescence quantum yields can reach 0.7. 40-42 On the contrary, upon aggregation most Pcs form nonfluorescent H-aggregates. We and others have previously demonstrated that functionalization of phthalocyanines with various biomolecules decreased their propensity to aggregate. 35-37,43 Nevertheless, in the absence of the binding target, Pcs remain aggregated and, therefore, are completely dark (non-fluorescent). When an H-aggregated Pc sensor molecule functionalized with a target-specific recognition group binds to a biomolecular target, it is pulled away from the aggregate, resulting in the Pc's de-aggregation leading to restoring its fluorescent emission. The ability of the Pc sensor to respond selectively on the binding to a specific target vs. non-selective binding to other biomolecules is generally controlled by the fine balance between the energy of the recognition group selective binding to the target biomolecule vs. interactions of the individual Pc molecule with aqueous environment (which can be controlled by a proper choice of solubilizing groups). Therefore, with a judicious molecular design, Pc aggregation/de-aggregation signal generation mechanism can be promising for intracellular imaging of biomolecular targets in the near-IR spectral range, and offers high S/B ratios while requiring no washes of unbound species. Previously, we have successfully demonstrated the application of the aggregation/de-aggregation principle for turn-on near-IR detection of oligonucleotide³⁵⁻³⁷ and protein targets³⁴ in *in vitro* and non-cellular environments.

In this work, we designed, prepared, characterized and demonstrated performance of a new Pc-based near-IR fluorescent sensors for wash-free high-contrast fluorescent imaging of a specific biomolecular target inside cells. The new sensing system enables high specificity and affinity of target recognition due to the use of an inhibitor-derived "anchor" unit coupled together with an aggregation/de-aggregation mechanism for fluorescent signal generation. For a proof-of-concept demonstration, we developed a sensor targeting the epidermal growth factor receptor (EGFR) tyrosine kinase in live and fixed cellular environments. The EGFR tyrosine kinase is a principal target for the ongoing search for potent anticancer therapeutics, and serves to illustrate the need to develop high efficiency imaging methods for the biomarker present within complex biological systems such as live cells. 44-50

Experimental Section

Below is the brief description of materials and experimental procedures. The detailed information is included in the *Supporting Information*.

Materials and reagents. All materials and reagents were obtained from established commercial suppliers.

Synthesis of the new sensor compound 2 (Scheme 1). Utilization of the solid-phase synthesis in the preparation of the ZnPc building block 5 is the key for obtaining the required mono-substituted phthalocyanine core. Thus, condensation of polymer resin-supported phthalonitrile 3 with excess phthalonitrile 4 yields a resin-attached ZnPc 5, followed by cleavage from the resin support to give mono-functionalized Pc building block 5. Subsequent coupling of 5 with the

"anchor" unit **6** furnishes the target sensor compound **2**. The detailed synthesis procedures and characterization of compounds **2**, **4**, **5** and other key intermediates are included in *Figures S5* – *S9*. The synthesis of compound **1** is described elsewhere.³⁴

EGFR kinase/sensor 2 binding in cell-free environments. EGFR kinase was reconstituted in buffer consisting of 50 mM HEPES, 20 mM MgCl₂, 100 μM MnCl₂, and 200 μM Na₃VO₄ at pH 7.4. Sensor 2 stock solutions were prepared in DMSO. The appropriate amounts of sensor 2 were added to the reconstituted EGFR kinase to yield 1% of DMSO in the final preparation. Emission measurements were started right after sample preparation. Excitation was set at 665 nm, while emission was collected from 680 to 750 nm.

Cellular imaging studies. We used A549 cell line (ATCC, CCL-185). Cells were thawed from liquid nitrogen storage and re-suspended with 9 mL F-12K Ham medium supplemented with 10% Fetal Bovine Serum (FBS) and 1% Antibiotic-Antimycotic. Cells were cultured in a humidified 37 °C incubator with 5% CO $_2$ atmospheric control. For sensor uptake, cells were plated at 1×10^5 cells/well for 6-well plates and at 3.15×10^3 cells/well for 96-well plates and incubated for 24 hours. Before the uptake, the growth medium in each well was refreshed and either sensor 1, sensor 2 (to yield a final concentration of $2-5~\mu\text{M}$), or 1% DMSO as a vehicle control was added to respective wells, and the cells were incubated for 0.5-24~h at 37 °C and 5 % CO $_2$. Imaging was performed on a Keyence BZ-800 fluorescent microscope with Chroma Technologies filter sets. All images were taken with a $60\times$ oil immersion objective.

Organelle tracker experiments. Following sensor **2** uptake, PBS wash, and media replacement, cells were treated singly or in combination with the following trackers: MitoTracker Green at 100 nM, DAPI at 1 ng/mL, LysoTracker at 50 nM, ER Tracker Green at 1 μM , or Golgi tracker NBD-C6 Ceramide at 10 μM concentration.

Immunocytochemistry. Following sensor's uptake, the cells were fixed and permeabilized with 3.7% formaldehyde and 0.18% Triton-X solution in PBS for 10 min at 37 °C. After PBS wash, the cells and growth surface were coated with blocking solution (1% BSA in PBS) for 30 min at 37 °C; and the cells were incubated with primary mouse anti-EGF receptor antibody in blocking solution, overnight, at 4 °C. The following day, unbound primary antibody was removed with three 5 min PBS washes; and the cells were incubated with goat antimouse IgG, Alexa Fluor™ 488-conjugated secondary antibody (1:2000) for 1 hour at room temperature. Unbound secondary antibody was removed with three additional 5-min PBS washes upon gentle rocking.

Results and Discussion

Sensor design and structure - cell bioavailability correlations.

Recently, we have developed a Pc sensor compound 1 (Scheme 1).³⁴ In cell-free and *in vitro* conditions, this compound acts as a selective turn-on fluorescent sensor for EGFR tyrosine kinase. The molecular structure of 1 consists of two domains: a target-binding "anchor" and a linked phthalocyanine (Pc) fluorescent reporter. The recognition "anchor" domain is related to the structure of gefitinib, an inhibitor that binds to the intracellular domain of EGFR tyrosine kinase (i.e. ATP binding pocket)^{51, 52} with high affinity ($K_d \sim 0.5$ -2 nM)⁵³ and selectivity.⁵⁴ The emissive reporter domain incorporates a ZnPc core known for the near-IR absorption/emission with high extinction coefficients and quantum yields.^{39-42, 55}. In aqueous environments, ZnPc aggregation leads to the non-emissive H-aggregate

state. In the presence of nanomolar concentrations of EGFR kinase, the "anchor's" selective binding to the target kinase causes partial deaggregation of ZnPc fluorophore and generation of the near-IR fluorescent emission in a concentration – dependent manner. At the same time, sensor 1 does not show non-selective binding and displays no fluorescent response to other biomacromolecules. Despite the promising performance of 1 in cell-free environments, transition to cellular imaging encountered major obstacles. First, we found that 1 was insufficiently water-soluble. Indeed, the *in vitro* target response experiments required an aqueous medium with 10 % DMSO to produce a fluorescent signal. Such conditions are obviously not ideal (if even achievable) for live-cell imaging. Second, intracellular bioavailability of 1 is rather low (discussed below). Simply increasing aqueous solubility via attaching better solubilizing groups to the hydrophobic ZnPc core proved ineffective as the in-

creasing hydrophilicity of ZnPc unit would interfere with the fine aggregation/de-aggregation balance required for proper operation of the emissive signal generation mechanism. High aqueous solubility would also diminish cell bioavailability of the sensor. To balance both aqueous solubility and bioavailability, while minimizing the interference with the aggregation/de-aggregation signal generation mechanism, we carefully redesigned the sensor 1 to include the same binding "anchor" domain but to modify the solubilizing side groups. After a series of less successful structural variations, we arrived at sensor 2. In this compound, incorporating cationic trimethylammonium groups attached at the ZnPc chromophore moderately enhances solubility and increases bioavailability, 39 while diethylene glycol framework of the solubilizing groups ensures effective operation of the aggregation/de-aggregation signal generation mechanism.

Scheme 1. Structure of the EGFR tyrosine kinase sensors 1 and 2, and synthesis of the sensor compound 2. Reagents and conditions: (a) Zn(OAc)₂, DBU, *n*-BuOH, DMF, 106 °C, 24 h; (b) TFA, CH₂Cl₂, 8 h; (c) HOBt, HBTU, DIPEA, DMF, 12 h.

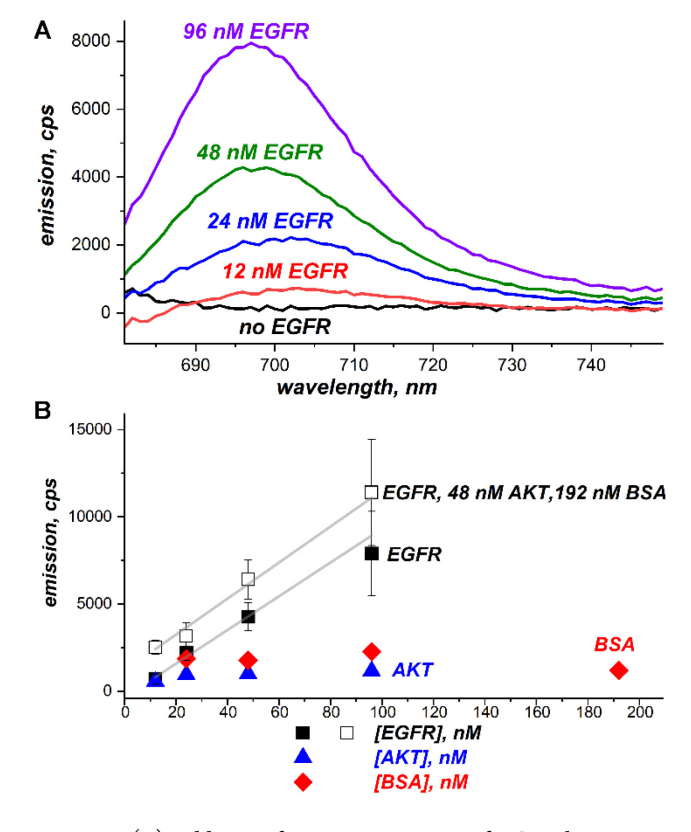


Figure 1. (A) Addition of increasing amount of EGFR kinase to a solution of sensor **2** results in a turn-on fluorescent response (no fluorescence is detected in the absence of EGFR kinase). Experimental conditions: concentration of sensor **2** 400 nM in 1% DMSO in aqueous buffer (50 mM HEPES, 20 mM MgCl₂, 100 μ M MnCl₂, and 200 μ M Na₃VO₄ at pH 7.4); excitation wavelength 665 nm; the spectra were corrected for the buffer background. (B) Sensor **2** shows linear fluorescent response to increasing EGFR concentration both in buffer (filled squares, adj. R^2 = 0.95) and in the presence of 48 nM AKT and 192 nM BSA (empty squares, adj. R^2 = 0.97). When added alone, AKT kinase (triangles) and BSA (diamonds) do not produce increase in emission intensity with increasing concentration.

The spectroscopic studies of 2 in the non-aggregated state (as a dilute solution in DMSO) reveal absorption and emission in the near-IR range (Figure S1 in the Supporting Information). It displays a high extinction coefficient (108,000 M⁻¹ cm⁻¹ at 681 nm) and a strong fluorescent emission at 690 nm (quantum yield in DMSO 0.23). In contrast to the previous sensor 1 (which requires 10% DMSO co-solvent for EGFR detection), the new sensor compound 2 can effectively operate under acceptable for live cells 1 % DMSO conditions. In aqueous EGFR kinase-free environments, due to ZnPc chromophore aggregation, sensor 2 displays no detectable fluorescence (Figure 1A). Monitoring of the fluorescent signal in aqueous conditions upon addition of EGFR kinase indicates that 2 responds quantitatively in a linear fashion to the changes in EGFR concentration (within nanomolar range, with LOD of 2 nM, filled squares in Figure 1B). It is noteworthy that the emission band maximum in aqueous conditions is bathochromically shifted compared to the corresponding spectrum in DMSO (to about 700 nm), which makes it even more suitable for near-IR imaging applications. The linearity of the fluorescent response on increasing EGFR kinase concentration is particularly valuable when quantitative analysis of EGFR kinase expression is required as part of the imaging process.

Other proteins, such as BSA and AKT kinase, do not produce a characteristic concentration-dependent response profile (triangles and diamonds in Figure 1B). At the same time, sensor **2** produces the concentration-dependent response to EGFR even over simultaneously present AKT and BSA background (Figure 1B, empty squares) with the linear regression slope (113 \pm 13) close to the one without AKT/BSA background (97 \pm 10). This reflects selective binding of the sensor **2** to EGFR kinase and selective turn-on fluorescent response on such binding.

Next, we evaluate whether the implemented structural modifications in 2 resulted in its increased bioavailability. As a model system, we choose the A549 cell line with a diffusion-mediated cellular uptake. A549 cells are human lung carcinoma cells with the high EGFR expression levels known both from the published work⁵⁶⁻⁵⁸ and also evaluated by us (Figure S2 in the Supporting Information). Individually, both modules of the sensor 2 - the "anchor" group and the ZnPc fluorescent unit - are cell membrane permeable. Indeed, the "anchor" parent structure, gefitinib, is an established anticancer drug, which was extensively characterized to be active intracellularly, and is a core structure for intracellular PET tracers. 51, 54, 59-68 Phthalocyanine compounds are also well positioned to enter cells, 39, 69-74 including the A549 line.⁷⁵ Therefore, we expect that the sensor compound 2 consisting of these two units linked together could also readily transfect inside the cells where it would selectively bind to intracellular EGFR kinase and generate a turn-on fluorescent signal via the aggregation/de-aggregation mechanism.

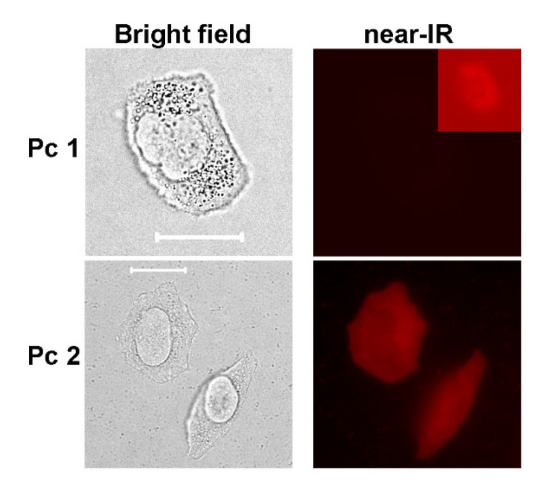


Figure 2. A549 cells exposed to 5 μM solutions of sensors 1 and 2 for 3 hours. Notice the low intensity of the near-IR signal with sensor 1, as compared to the much higher intensity with sensor 2. The conditions for uptake, imaging, and post-processing image treatment were identical for all images; all the experiments were performed using the same setup. The cells were fixed prior to imaging. Insert: "exposure", deliberately increased by image processing software, shows a weak emissive signal from a cell. Insert scale (reduced: original): 1:2.5. White scale bars in the bright field images correspond to 20 μm .

To confirm the better bioavailability of the structurally modified sensor 2, we compare near-IR fluorescent images upon exposing AS49 cells to the sensors 1 and 2 under identical conditions (5 μM sensor solution in 1 % DMSO in cell growth media, Figure 2). For fluorescent microscopy, we use a narrow-band red filter with the transmission maximum at 650 nm in the excitation channel, and a

narrow transmission band filter with the maximum at 720 nm in the emission channel. We observe significantly higher near-IR emission intensities for the sensor **2**, which produces fluorescent images with a much improved contrast, indicating that the implemented structural modifications in **2** do result in its increasing uptake by A549 cells (Figure 2).

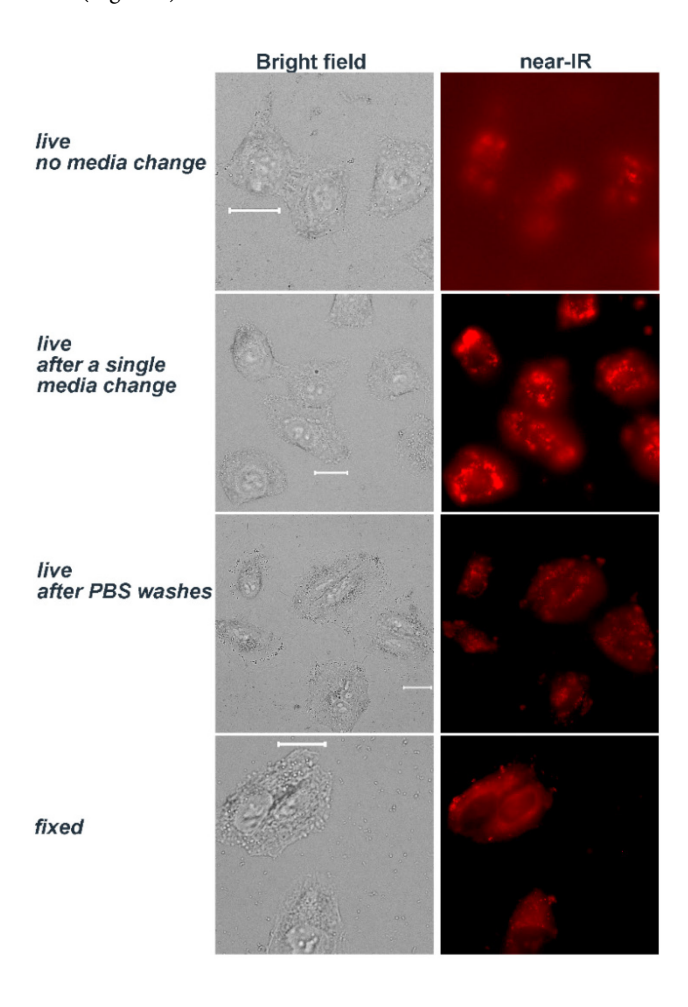


Figure 3. Typical images of live and fixed cells after exposure to $5\,\mu M$ solution of sensor 2 for 3 hours under different treatment protocols. "Live without media change": sensor 2 is added to cells; and cells are imaged after the exposure in the same environment. "Live after a single media change": sensor 2 is added to cells; media is changed after exposure; and cells are imaged in media. "Live after PBS washes": sensor 2 is added to cells; cells are washed with PBS after the exposure; and cells are imaged in media. "Fixed": sensor 2 is added to cells; fixation protocol is applied after the exposure time; and cells are imaged in PBS. White scale bars in bright field images correspond to 20 μ m.

We also confirm that the small molecule sensor 2 is suitable for imaging cells under various treatment protocols: live cells without washes or media changes, live cells with PBS washes, and fixed cells (Figure 3). However, we notice that whereas the sensor distribution patterns in fixed and live cells (under all treatment variations) look similar, more haziness appears in the fixed cells while live cells show a more punctate emission distribution. The slight variation of the distribution patterns between live and fixed cells could be due to the factors unrelated to the sensor (e.g. different stages of the cell cycle, disruptions due to imaging time outside of the incubator, redistribution of the EGFR upon cell fixation, etc.). Further investigation of

the differences in distribution patterns is outside of the scope of this report.

Cell uptake and imaging properties. First, to establish safe uptake conditions, we evaluate A549 cell viability in the presence of varying concentrations $(0 - 10 \mu M)$ of sensor 2 for up to 72 hours using an MTT (3-(4,5-dimethylthiazol-2-yl)-2,5-diphenyltetrazolium bromide) assay. An MTT assay assesses cell metabolic activity under various challenges including exposure to extrinsic agents (sensor 2 in our case). If the exposure influences cell metabolic activity, the colorimetric response of the MTT reagent differs from a baseline (cells that are not exposed to an agent). Our observations (Figure 4) indicate that the cell metabolic activity upon a 72-hour exposure even to the highest 10 μM concentration of **2** is not appreciably different from the control (cells that have not been exposed to 2). Interestingly, our results correlate very well with the previous reports on resistance of A549 cells towards 10 – 20 µM levels of gefitinib, ⁷⁶ a parent structure of the sensor 2. Thus, a 72-hour exposure to sensor 2 at concentrations up to 10 µM is not toxic to A549 cells.

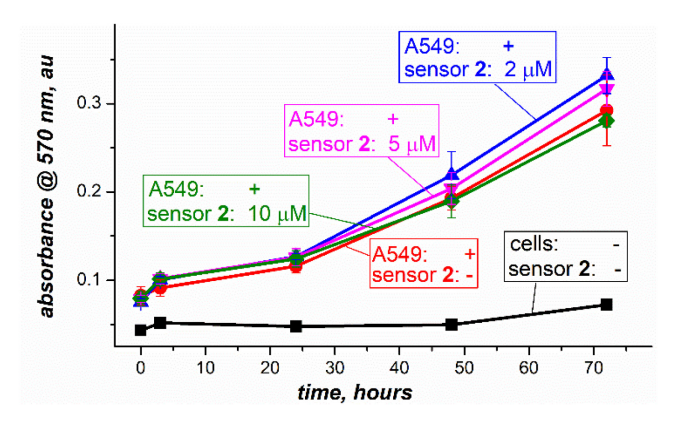


Figure 4. MTT assay indicates that the exposure of A549 cells to $2-10~\mu M$ concentrations of sensor $\boldsymbol{2}$ for up to 72 hours (blue up-pointing triangles $(2~\mu M)$, magenta down-pointing triangles $(5~\mu M)$, green diamonds $(10~\mu M))$ does not cause detectable changes in cells' metabolic activity compared to control (cells that have not been exposed to $\boldsymbol{2}$, red circles). MTT absorption does not change over the same period in the absence of cells (black squares).

Next, to optimize cellular uptake conditions, we expose the A549 cells to sensor 2 within the time and concentration limits established via the MTT assay. We find that the $3.5 - 5 \mu M$ concentration range enables the brightest emission (Figure S3 in the Supporting Information). Expectedly, when A549 cells are incubated with the 5 μM solution of sensor 2 for various times (ranging within 0.5 -24 hours), we observe that the near-IR channel emission is brighter at longer incubation times (Figure S4). At the same time, at longer incubation times, we also observe intensification of bright clusterlike background interferences outside of cell boundaries (appearing as red spots on the fluorescent images at 24-hour incubation, encircled in Figure S4). At this point, we do not know the true nature of the interference but hypothesize that at higher concentrations sensor 2 may cluster on cell debris: EGFR tyrosine kinase protein localizes on cellular membrane; therefore, the cell debris expose multiple sites available to bind sensor 2. It should be emphasized that, based

on the MTT results (discussed above), the higher concentrations of sensor **2** are not toxic to A549 cells. Nevertheless, to minimize potential interferences with imaging, we proceed with incubations not exceeding 3 hours in subsequent experiments.

Intracellular localization. We evaluate the sensor's **2** intracellular localization with focus on two goals: (i) to address a potential concern that large hydrophobic compounds like **2** could unselectively stain membranes of intracellular organelles,²⁹ and (ii) to demonstrate the sensor **2** co-localization with the target intracellular EGFR tyrosine kinase.

When we overlay fluorescent emission of sensor 2 with the emission from standard organelle trackers DAPI (nucleus), Mito (mitochondria), Lyso (lysosomes), ER (Endoplasmic reticulum), and Golgi apparatus (Figure 5), we do not observe any appreciable overlaps between the distribution of 2 and either of the trackers. Since organelle trackers do not display particular selectivity for any specific biomacromolecular targets, we conclude that sensor 2 does not unselectively stain the respective organelles and their membranes.

Finally, to prove the selectivity of EGFR tyrosine kinase imaging with sensor 2, we demonstrate its co-localization with EGFR kinase inside the cells via immunofluorescent experiments. In this study, we first incubate live A549 cells with sensor 2, fix, then permeabilize and stain the cells with an EGFR-specific primary antibody followed by fluorescently-tagged with Alexa Fluor™ 488 secondary antibody (Figure 6). When overlaying the images, we observe a substantial overlap of green (Alexa Fluor™ 488 antibody label) and near-IR (sensor 2) channel emissions, with Pearson correlation coefficient of 0.92 ±0.01. The good overlap convincingly indicates that sensor 2 indeed co-localizes with EGFR tyrosine kinase inside the cells, and, therefore, can be used for selective fluorescent imaging of the intracellular protein distribution. In contrast to antibody-based fluorescent immunoassays which can only be performed with fixed cells, sensor 2 enables simple and selective imaging and visualization of

EGFR tyrosine kinase distribution in live cells, which can be used for EGFR monitoring via fluorescent microscopy and development of cell-based fluorescent assays for high throughput screening of EGFR kinase inhibitors.

Conclusions

We designed and validated a new type of small-molecule-based near-IR fluorescent sensing system for intracellular imaging and quantitation of biomacromolecular targets. The sensor's turn-on fluorescent response is based on the novel phthalocyanine aggregation/de-aggregation mechanism, while its high selectivity stems from the presence of a strong inhibitor scaffold as a target-recognition domain. This is the first report of using Pc aggregation/de-aggregation based system for cellular imaging of a specific protein target.

The reported sensing platform demonstrates typical for the near-IR spectral range high S/B ratios and eliminates the need for using multiple reagents, covalent intra-cell assembly, and post-exposure washes. The latter is the key condition for observing and evaluating biomolecules in their true native environments. As a proof-of-concept, we develop the sensor 2 specifically targeting EGFR tyrosine kinase and demonstrate the selective and sensitive near-IR fluorescent imaging of this protein inside live and fixed cells with a range of treatment protocols including ones with no washes. While we do acknowledge a potential possibility of non-specific binding of phthalocyanine fragments over hydrophobic regions of biomacromolecules (resulting in phthalocyanine de-aggregation), the magnitude of this phenomenon appears insignificant as demonstrated via extensive organelle tracker experiments and *in vitro* specificity studies

We expect that the new general sensor design principles, structure/bioavailability correlation, and the modular structure of the sensing system can be extended towards selective fluorescent imaging of other important biomacromolecular targets.

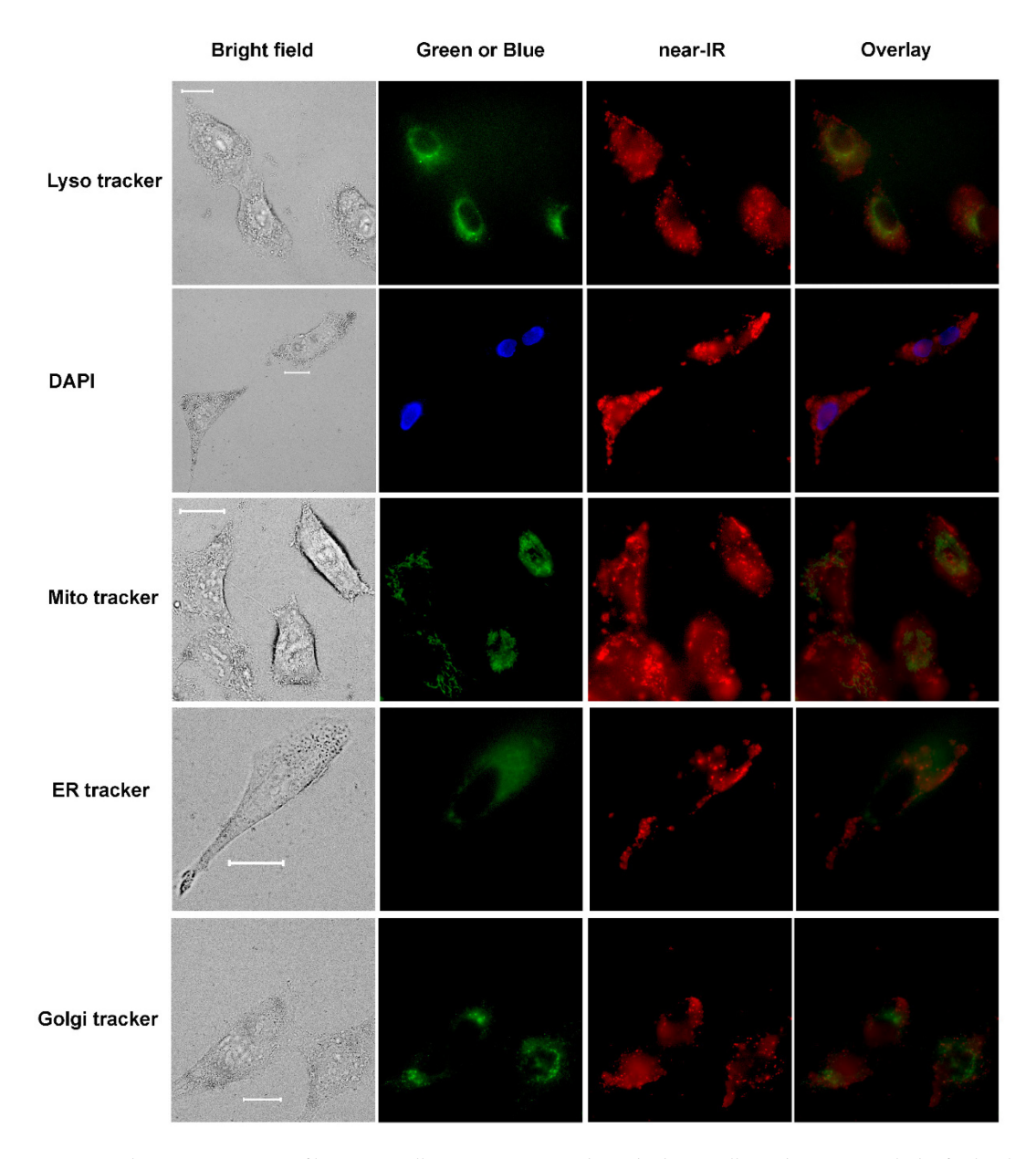


Figure 5. Fluorescent imaging of live A549 cells using sensor ${\bf 2}$ and standard organelle trackers. Notice lack of colocalization in the near-IR channel (sensor ${\bf 2}$) with the green or blue channels. Experimental conditions: 5 μ M solution of sensor ${\bf 2}$ in 1% DMSO in media (exposure time 3 hours); 2 μ M of Mito tracker or 1 ng/mL DAPI or 1 μ M Lyso tracker or 1 μ M of ER tracker or 10 μ M of Golgi tracker. Exposure time to organelle trackers is included in the experimental protocol (Supporting Information). White scale bars in bright field images correspond to 20 μ m.

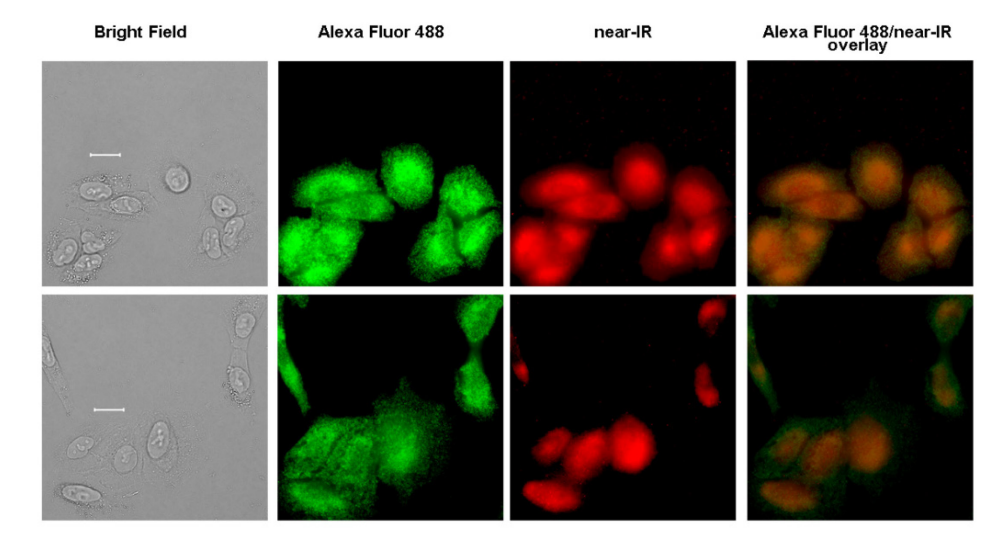


Figure 6. Fluorescent imaging of A549 cells demonstrating sensor $\bf 2$ colocalization with EGFR specific antibody. Notice substantial overlap of the images in green (fluorescent antibody) and near-IR channels (sensor $\bf 2$). Experimental conditions: 5 μ M sensor $\bf 2$ in 1% DMSO in aqueous buffer, exposure for 3 hours, fixed cells, post-fixation antibody staining. White scale bars in bright field images correspond to 20 μ m.

ASSOCIATED CONTENT

Supporting Information. Materials, synthetic procedures and experimental protocols, Figures S1-S10. This material is available free of charge via the Internet at http://pubs.acs.org.

AUTHOR INFORMATION

Corresponding Author

* Evgueni E. Nesterov (<u>een@niu.edu</u>), Irina V. Nesterova (<u>inesterova@niu.edu</u>).

ACKNOWLEDGMENT

This research was supported by the National Institute of General Medical Sciences of the National Institutes of Health under the award number 1R15GM140403-01. Purchase of the NMR spectrometer used to obtain results included in this publication was supported by the National Science Foundation under the MRI award CHE-2117776. We acknowledge the Northern Illinois University's BIOS Research Instrumentation Core (directed by Professor Barrie P. Bode) for support of cellular experiments.

REFERENCES

- (1) Han, H.-H.; Tian, H., Jr.; Zang, Y.; Sedgwick, A. C.; Li, J.; Sessler, J. L.; He, X.-P.; James, T. D. Small-Molecule Fluorescence-Based Probes for Interrogating Major Organ Diseases. *Chem. Soc. Rev.* **2021**, *50* (17), 9391-9429.
- (2) Morris, M. C. Spotlight on Fluorescent Biosensors-Tools for Diagnostics and Drug Discovery. ACS Med. Chem. Lett. **2014**, 5 (2), 99-101.
- (3) Han, H.-H.; Sedgwick, A. C.; Shang, Y.; Li, N.; Liu, T.; Li, B.-H.; Yu, K.; Zang, Y.; Brewster, J. T.; Odyniec, M. L.; et al. Protein Encapsulation: a New Approach for Improving the Capability of Small-Molecule Fluorogenic Probes. *Chem. Sci.* **2020**, *11* (4), 1107-1113.
- (4) Sheng, W.; Nick, S. T.; Santos, E. M.; Ding, X.; Zhang, J.; Vasileiou, C.; Geiger, J. H.; Borhan, B. A Near-Infrared Photoswitchable Protein-Fluorophore Tag for No-Wash Live Cell Imaging. *Angew. Chem., Int. Ed.* **2018**, *57* (49), 16083-16087.

- (5) Carlson, J. C. T.; Meimetis, L. G.; Hilderbrand, S. A.; Weissleder, R. BODIPY-Tetrazine Derivatives as Superbright Bioorthogonal Turn-on Probes. *Angew. Chem.,Int. Ed.* **2013**, 52 (27), 6917-6920.
- (6) Meimetis, L. G.; Carlson, J. C. T.; Giedt, R. J.; Kohler, R. H.; Weissleder, R. Ultrafluorogenic Coumarin-Tetrazine Probes for Real-Time Biological Imaging, *Angew. Chem., Int. Edit.* **2014**, 53 (29), 7531-7534.
- (7) Wieczorek, A.; Werther, P.; Euchner, J.; Wombacher, R. Green- to Far-Red-Emitting Fluorogenic Tetrazine Probes Synthetic Access and No-Wash Protein Imaging Inside Living Cells. *Chem. Sci.* **2017**, 8 (2), 1506-1510.
- (8) Yuan, L.; Wang, L.; Agrawalla, B. K.; Park, S.-J.; Zhu, H.; Sivaraman, B.; Peng, J.; Xu, Q.-H.; Chang, Y.-T. Development of Targetable Two-Photon Fluorescent Probes to Image Hypochlorous Acid in Mitochondria and Lysosome in Live Cell and Inflamed Mouse Model. *J. Am. Chem. Soc.* **2015**, *137* (18), 5930-5938.
- (9) Modi, S.; Nizak, C.; Surana, S.; Halder, S.; Krishnan, Y. Two DNA Nanomachines Map pH Changes Along Intersecting Endocytic Pathways Inside the Same Cell. *Nat. Nanotechnol.* **2013**, *8* (6), 459-467.
- (10) Modi, S.; Swetha, M. G.; Goswami, D.; Gupta, G. D.; Mayor, S.; Krishnan, Y. A DNA Nanomachine That Maps Spatial and Temporal pH Changes Inside Living Cells. *Nat. Nanotechnol.* **2009**, 4 (5), 325-330.
- (11) Chakraborty, K.; Veetil, A. T.; Jaffrey, S. R.; Krishnan, Y. Nucleic Acid-Based Nanodevices in Biological Imaging. *Annu. Rev. Biochem.* **2016**, 85, 349-373.
- (12) Qian, L. H.; Pan, S.; Lee, J. S.; Ge, J.; Li, L.; Yao, S. Q. Live-Cell Imaging and Profiling of c-Jun N-Terminal Kinases Using Covalent Inhibitor-Derived Probes. *Chem. Commun.* **2019**, *55* (8), 1092-1095.
- (13) Shao, Y.; Zhao, J.; Yuan, J.; Zhao, Y.; Li, L. Organelle-Specific Photoactivation of DNA Nanosensors for Precise Profiling of Subcellular Enzymatic Activity. *Angew. Chem., Int. Ed.* **2021**, *60* (16), 8923-8931.
- (14) Li, L.; Zhang, C. W.; Ge, J. Y.; Qian, L. H.; Chai, B. H.; Zhu, Q.; Lee, J. S.; Lim, K. L.; Yao, S. Q. A Small-Molecule Probe for Selective Profiling and Imaging of Monoamine OxidaseB Activities in Models of Parkinson's Disease. *Angew. Chem., Int. Ed.* **2015**, 54 (37), 10821-10825.
- (15) Fleming, C. L.; Sandoz, P. A.; Inghardt, T.; Öenfelt, B.; Grøtli, M.; Andréasson, J. A Fluorescent Kinase Inhibitor that Exhibits Diagnostic Changes in Emission upon Binding. *Angew. Chem., Int. Ed.* **2019**, 58 (42), 15000-15004.
- (16) Alamudi, S. H.; Chang, Y. T. Advances in the Design of Cell-Permeable Fluorescent Probes for Applications in Live Cell Imaging. *Chem. Commun.* **2018**, *54* (97), 13641-13653.

- (17) Wu, Q.; Jing, Y.; Zhao, T.; Gao, J.; Cai, M.; Xu, H.; Liu, Y.; Liang, F.; Chen, J.; Wang, H. Development of Small Molecule Inhibitor-Based Fluorescent probes for Highly Specific Super-Resolution Imaging. *Nanoscale* **2020**, *12* (42), 21591-21598.
- (18) Heilemann, M.; van de Linde, S.; Schüttpelz, M.; Kasper, R.; Seefeldt, B.; Mukherjee, A.; Tinnefeld, P.; Sauer, M. Subdiffraction-Resolution Fluorescence Imaging with Conventional Fluorescent Probes. *Angew. Chem., Int. Ed.* **2008**, 47 (33), 6172-6176.
- (19) Yang, K. S.; Budin, G.; Reiner, T.; Vinegoni, C.; Weissleder, R. Bioorthogonal Imaging of Aurora Kinase A in Live Cells. *Angew. Chem., Int. Ed.* **2012**, *51* (27), 6598-6603.
- (20) Huber, M. E.; Toy, L.; Schmidt, M. F.; Vogt, H.; Budzinski, J.; Wiefhoff, M. F. J.; Merten, N.; Kostenis, E.; Weikert, D.; Schiedel, M. A Chemical Biology Toolbox Targeting the Intracellular Binding Site of CCR9: Fluorescent Ligands, New Drug Leads and PROTACs. *Angew. Chem., Int. Ed.* **2022**, *61* (12), e202116782.
- (21) Gioux, S.; Choi, H. S.; Frangioni, J. V. Image-Guided Surgery Using Invisible Near-Infrared Light: Fundamentals of Clinical Translation. *Mol. Imaging* **2010**, *9* (5), 237-255.
- (22) Soper, S. A.; Mattingly, Q. L.; Vegunta, P. Photon Burst Detection of Single Near-Infrared Fluorescent Nolecules. *Anal. Chem.* **1993**, *65* (6), 740-747.
- (23) Williams, D. C.; Soper, S. A. Ultrasensitive Near-IR Fluorescence Detection for Capillary Gel-Electrophoresis and DNA-Sequencing Applications. *Anal. Chem.* **1995**, *67* (19), 3427-3432.
- (24) Frangioni, J. V. In vivo Near-Infrared Fluorescence Imaging. *Curr. Opin. Chem. Biol.* **2003**, *7* (5), 626-634.
- (25) Adams, K. E.; Ke, S.; Kwon, S.; Liang, F.; Fan, Z.; Lu, Y.; Hirschi, K.; Mawad, M. E.; Barry, M. A.; Sevick-Muraca, E. M. Comparison of Visible and Near-infrared Wavelength-excitable Fluorescent Dyes for Molecular Imaging of Cancer. *J. Biomed. Opt.* **2007**, *12* (2), 024017.
- (26) Cheng, K.; Chen, H.; Jenkins, C. H.; Zhang, G. L.; Zhao, W.; Zhang, Z.; Han, F.; Fung, J.; Yang, M.; Jiang, Y. X.; et al. Synthesis, Characterization, and Biomedical Applications of a Targeted Dual-Modal Near-Infrared-II Fluorescence and Photoacoustic Imaging Nanoprobe. *ACS Nano* **2017**, *11* (12), 12276-12291.
- (27) Shieh, P.; Bertozzi, C. R. Design Strategies for Bioorthogonal Smart Probes. Org. Biomol. Chem. **2014**, 12 (46), 9307-9320.
- (28) Zhuang, Y. D.; Chiang, P. Y.; Wang, C. W.; Tan, K. T. Environment-Sensitive Fluorescent Turn-On Probes Targeting Hydrophobic Ligand-Binding Domains for Selective Protein Detection. *Angew. Chem., Int. Ed.* **2013**, 52 (31), 8124-8128.
- (29) MacNevin, C. J.; Watanabe, T.; Weitzman, M.; Gulyani, A.; Fuehrer, S.; Pinkin, N. K.; Tian, X.; Liu, F.; Jin, J.; Hahn, K. M. Membrane-Permeant, Environment-Sensitive Dyes Generate Biosensors within Living Cells. *J. Am. Chem. Soc.* **2019**, *141* (18), 7275-7282.
- (30) Zhai, D. T.; Xu, W.; Zhang, L. Y.; Chang, Y. T. The Role of "Disaggregation" in Optical Probe Development. *Chem. Soc. Rev.* **2014**, 43 (8), 2402-2411.
- (31) Ren, C.; Zhang, J.; Chen, M.; Yang, Z. Self-assembling Small Molecules for the Detection of Important Analytes. *Chem. Soc. Rev.* **2014**, 43 (21), 7257-7266.
- (32) Shoemaker, R. H. The NCI60 human tumour cell line anticancer drug screen. *Nat. Rev. Cancer* **2006**, *6* (10), 813-823.
- (33) Michelini, E.; Cevenini, L.; Mezzanotte, L.; Coppa, A.; Roda, A. Cell-based assays: fuelling drug discovery. *Anal. Bioanal. Chem.* **2010**, 398 (1), 227-238.
- (34) Ducharme, G. T.; LaCasse, Z.; Sheth, T.; Nesterova, I. V.; Nesterov, E. E. Design of Turn-On Near-Infrared Fluorescent Probes for Highly Sensitive and Selective Monitoring of Biopolymers. *Angew. Chem., Int. Ed.* **2020**, *59* (22), 8440-8444.
- (35) Nesterova, I. V.; Bennett, C. A.; Erdem, S. S.; Hammer, R. P.; Deininger, P. L.; Soper, S. A. Near-IR Single Fluorophore Quenching System Based on Phthalocyanine (Pc) Aggregation and its Application for

- Monitoring Inhibitor/Activator Action on a Therapeutic Target: L1-EN. *Analyst* **2011**, *136* (6), 1103-1105.
- (36) Nesterova, I. V.; Erdem, S. S.; Pakhomov, S.; Hammer, R. P.; Soper, S. A. Phthalocyanine Dimerization-Based Molecular Beacons Using Near-IR Fluorescence. *J. Am. Chem. Soc.* **2009**, *131* (7), 2432-2433.
- (37) Nesterova, I. V.; Verdree, V. T.; Pakhomov, S.; Strickler, K. L.; Allen, M. W.; Hammer, R. P.; Soper, S. A. Metallo-Phthalocyanine Near-IR Fluorophores: Oligonucleotide Conjugates and Their Applications in PCR Assays. *Bioconjugate Chem.* **2007**, 18 (6), 2159-2168.
- (38) Lebedeva, N. S. Aggregation Properties of Water-Soluble Metal Phthalocyanines: Effect of Ionic Strength of Solution. *Russ. Chem. Bull.* **2004**, 53 (12), 2674-2683.
- (39) Ongarora, B. G.; Hu, X. K.; Verberne-Sutton, S. D.; Garno, J. C.; Vicente, M. G. H. Syntheses and Photodynamic Activity of Pegylated Cationic Zn(II)-Phthalocyanines in HEp2 Cells. *Theranostics* **2012**, 2 (9), 850-870.
- (40) Escobedo, J. O.; Rusin, O.; Lim, S.; Strongin, R. M. NIR Dyes for Bioimaging Applications. *Curr. Opin. Chem. Biol.* **2010**, *14* (1), 64-70.
- (41) Ogunsipe, A.; Nyokong, T. Effects of Substituents and Solvents on the Photochemical Properties of Zinc Phthalocyanine Complexes and Their Protonated Derivatives. *J. Mol. Struct.* **2004**, *689* (1-2), 89-97.
- (42) Ogunsipe, A.; Maree, D.; Nyokong, T. Solvent Effects on the Photochemical and Fluorescence Properties of Zinc Phthalocyanine Derivatives. *J. Mol. Struct.* **2003**, *650* (1-3), 131-140.
- (43) Duan, W. B.; Smith, K.; Savoie, H.; Savoie, H.; Greenman, J.; Boyle, R. W. Near IR Emitting Isothiocyanato-Substituted Fluorophores: Their Synthesis and Bioconjugation to Monoclonal Antibodies. *Org. Biomol. Chem.* **2005**, 3 (13), 2384-2386.
- (44) Gonzalez de Castro, D.; Clarke, P. A.; Al-Lazikani, B.; Workman, P. Personalized Cancer Medicine: Molecular Diagnostics, Predictive biomarkers, and Drug Resistance. *Clin. Pharmacol. Ther.* **2013**, 93 (3), 252-259.
- (45) Heist, R. S.; Christiani, D. EGFR-Targeted Therapies in Lung Cancer: Predictors of Response and Toxicity. *Pharmacogenomics* **2009**, *10* (1), 59-68.
- (46) Ji, H.; Sharpless, N. E.; Wong, K. K. EGFR Targeted Therapy: View from Biological Standpoint. *Cell cycle (Georgetown, Tex.)* **2006**, *S* (18), 2072-2076.
- (47) Mendelsohn, J.; Baselga, J. The EGF Receptor Family as Targets for Cancer Therapy. *Oncogene* **2000**, 19 (56), 6550-6565.
- (48) Mendelsohn, J.; Baselga, J. Status of Epidermal Growth Factor Receptor Antagonists in the Biology and Treatment of Cancer. *J. Clin. Oncol.* **2003**, *21* (14), 2787-2799.
- (49) Pao, W.; Chmielecki, J. Rational, Biologically Based Treatment of EGFR-Mutant Non-Small-Cell Lung Cancer. *Nat. Rev. Cancer* **2010**, *10* (11) 760-774
- (50) Kaufman, N. E. M.; Dhingra, S.; Jois, S. D.; Vicente, M. d. G. H. Molecular Targeting of Epidermal Growth Factor Receptor (EGFR) and Vascular Endothelial Growth Factor Receptor (VEGFR). *Molecules* **2021**, 26 (4), 1076.
- (51) Ortu, G.; Ben-David, I.; Rozen, Y.; Freedman, N. M. T.; Chisin, R.; Levitzki, A.; Mishani, E. Labeled EGFr-TK Irreversible Inhibitor (ML03): In Vitro and In Vivo Properties, Potential as PET Biomarker for Cancer and Feasibility as Anticancer Drug. *Int. J. Cancer* **2002**, *101* (4), 360-370.
- (52) Wakeling, A. E.; Guy, S. P.; Woodburn, J. R.; Ashton, S. E.; Curry, B. J.; Barker, A. J.; Gibson, K. H. ZD1839 (Iressa): an Orally Active Inhibitor of Epidermal Growth Factor Signaling with Potential for Cancer Therapy. *Cancer Res.* **2002**, *62* (20), 5749-5754.
- (53) Davis, M. I.; Hunt, J. P.; Herrgard, S.; Ciceri, P.; Wodicka, L. M.; Pallares, G.; Hocker, M.; Treiber, D. K.; Zarrinkar, P. P. Comprehensive Analysis of Kinase Inhibitor Selectivity. *Nat. Biotechnol.* **2011**, 29 (11), 1046-1051.
- (54) Abourbeh, G.; Dissoki, S.; Jacobson, O.; Litchi, A.; Ben Daniel, R.; Laki, D.; Levitzki, A.; Mishani, E. Evaluation of Radiolabeled ML04, a Putative Irreversible Inhibitor of Epidermal Growth Factor Receptor, as a

- Bioprobe for PET Imaging of EGFR-Overexpressing Tumors. *Nucl. Med. Biol.* **2007**, 34 (1), 55-70.
- (55) Verdree, V. T.; Pakhomov, S.; Su, G.; Allen, M. W.; Countryman, A. C.; Hammer, R. P.; Soper, S. A. Water Soluble Metallo-phthalocyanines: The Role of the Functional Groups on the Spectral and Photophysical Properties. *J. Fluoresc.* **2007**, *17* (5), 547-563.
- (56) Li, M. F.; Yang, J. L.; Zhang, L. H.; Tu, S. F.; Zhou, X.; Tan, Z.; Zhou, W. J.; He, Y. J.; Li, Y. H. A Low-Molecular-Weight Compound Exerts Anticancer Activity Against Breast and Lung Cancers by Disrupting EGFR/Eps8 Complex Formation. *J. Exp. Clin. Cancer Res.* **2019**, 38, 211.
- (57) Antczak, C.; Bermingham, A.; Calder, P.; Malkov, D.; Song, K. M.; Fetter, J.; Djaballah, H. Domain-Based Biosensor Assay to Screen for Epidermal Growth Factor Receptor Modulators in Live Cells. *Assay Drug Dev. Technol.* **2012**, *10* (1), 24-36.
- (58) Antczak, C.; Mahida, J. P.; Bhinder, B.; Calder, P. A.; Djaballah, H. A High-Content Biosensor-Based Screen Identifies Cell-Permeable Activators and Inhibitors of EGFR Function: Implications in Drug Discovery. J. Biomol. Screen 2012, 17 (7), 885-899.
- (59) Pal, A.; Glekas, A.; Doubrovin, M.; Balatoni, J.; Namavari, M.; Beresten, T.; Maxwell, D.; Soghomonyan, S.; Shavrin, A.; Ageyeva, L.; et al. Molecular Imaging of EGFR Kinase Activity in Tumors with ¹²⁴I-Labeled Small Molecular Tracer and Positron Emission Tomography. *Mol. Imaging Biol.* **2006**, 8 (5), 262-277.
- (60) Pal, A.; Balatoni, J. A.; Mukhopadhyay, U.; Ogawa, K.; Gonzalez-Lepera, C.; Shavrin, A.; Volgin, A.; Tong, W.; Alauddin, M. M.; Gelovani, J. G. Radiosynthesis and Initial In Vitro Evaluation of ^[18F]F-PEG₆-IPQA--a Novel PET Radiotracer for Imaging EGFR Expression-Activity in Lung Carcinomas. *Mol. Imaging Biol.* **2011**, *13* (5), 853-861.
- (61) Yeh, H. H.; Ogawa, K.; Balatoni, J.; Mukhapadhyay, U.; Pal, A.; Gonzalez-Lepera, C.; Shavrin, A.; Soghomonyan, S.; Flores, L., 2nd; Young, D.; et al. Molecular Imaging of Active Mutant L858R EGF Receptor (EGFR) Kinase-Expressing Nonsmall Cell Lung Carcinomas Using PET/CT. Proc. Natl. Acad. Sci. 2011, 108 (4), 1603-1608.
- (62) Mishani, E.; Hagooly, A. Strategies for Molecular Imaging of Epidermal Growth Factor Receptor Tyrosine Kinase in Cancer. *J. Nucl. Med.* **2009**, *50* (8), 1199-1202.
- (63) Mishani, E.; Abourbeh, G.; Eiblmaier, M.; Anderson, C. J. Imaging of EGFR and EGFR Tyrosine Kinase Overexpression in Tumors by Nuclear Medicine Modalities. *Curr. Pharm. Des.* **2008**, *14* (28), 2983-2998.
- (64) Mishani, E.; Abourbeh, G.; Rozen, Y.; Jacobson, O.; Laky, D.; Ben David, I.; Levitzki, A.; Shaul, M. Novel Carbon-11 Labeled 4-dimethylamino-but-2-enoic acid [4-(phenylamino)-quinazoline-6-yl]-amides: Potential PET Bioprobes for Molecular Imaging of EGFR-Positive Tumors. *Nucl. Med. Biol.* **2004**, *31* (4), 469-476.
- (65) Bonasera, T. A.; Ortu, G.; Rozen, Y.; Krais, R.; Freedman, N. M.; Chisin, R.; Gazit, A.; Levitzki, A.; Mishani, E. Potential ¹⁸F-Labeled Biomarkers for Epidermal Growth Factor Receptor Tyrosine Kinase. *Nucl. Med. Biol.* **2001**, 28 (4), 359-374.

- (66) Memon, A. A.; Jakobsen, S.; Dagnaes-Hansen, F.; Sorensen, B. S.; Keiding, S.; Nexo, E. Positron Emission Tomography (PET) Imaging with [¹¹C]-Labeled Erlotinib: A Micro-PET Study on Mice with Lung Tumor Xenografts. *Cancer Res.* **2009**, *69* (3), 873-878.
- (67) Dissoki, S.; Aviv, Y.; Laky, D.; Abourbeh, G.; Levitzki, A.; Mishani, E. The effect of the [18F]-PEG group on tracer qualification of [4-(phenylamino)-quinazoline-6-YL]-amide moiety—An EGFR putative irreversible inhibitor. *Appl. Radiat. Isot.* **2007**, *65* (10), 1140-1151.
- (68) Shaul, M.; Abourbeh, G.; Jacobson, O.; Rozen, Y.; Laky, D.; Levitzki, A.; Mishani, E. Novel Iodine-124 Labeled EGFR Inhibitors as Potential PET Agents for Molecular Imaging in Cancer. *Bioorg. Med. Chem.* **2004**, *12* (13), 3421-3429.
- (69) Liu, W.; Jensen, T. J.; Fronczek, F. R.; Hammer, R. P.; Smith, K. M.; Vicente, M. G. H. Synthesis and Cellular Studies of Nonaggregated Water-Soluble Phthalocyanines. *J. Med. Chem.* **2005**, *48* (4), 1033-1041.
- (70) Chan, W. S.; Svensen, R.; Phillips, D.; Hart, I. R. Cell Uptake, Distribution and Response to Aluminium Chloro Sulphonated Phthalocyanine, a Potential Anti-Tumour Photosensitizer. *Br. J. Cancer* **1986**, 53 (2), 255-263.
- (71) Sibrian-Vazquez, M.; Ortiz, J.; Nesterova, I. V.; Fernández-Lázaro, F.; Sastre-Santos, A.; Soper, S. A.; Vicente, M. G. H. Synthesis and Properties of Cell-Targeted Zn(II)—Phthalocyanine—Peptide Conjugates. *Bioconjugate Chem.* **2007**, *18* (2), 410-420.
- (72) Li, H. R.; Jensen, T. J.; Fronczek, F. R.; Vicente, M. G. H. Syntheses and Properties of a Series of Cationic Water-Soluble Phthalocyanines. *J. Med. Chem.* **2008**, *51* (3), 502-511.
- (73) Bai, M.; Lo, P. C.; Ye, J.; Wu, C.; Fong, W. P.; Ng, D. K. P. Facile Synthesis of Pegylated Zinc(II) Phthalocyanines via Transesterification and Their in Vitro Photodynamic Activities. *Org. Biomol. Chem.* **2011**, 9 (20), 7028-7032.
- (74) Liu, J.-Y.; Jiang, X.-J.; Fong, W.-P.; Ng, D. K. P. Highly Photocytotoxic 1,4-Dipegylated Zinc(ii) Phthalocyanines. Effects of the Chain Length on the In Vitro Photodynamic Activities. *Org. Biomol. Chem.* **2008**, *6* (24), 4560-4566.
- (75) Maduray, K.; Odhav, B. The *in vitro* Photodynamic Effect of Laser Activated Gallium, Indium and Iron Phthalocyanine Chlorides on Human Lung Adenocarcinoma Cells. *J. Photochem. Photobiol., B* **2013**, 128, 58-63.
- (76) Ono, M.; Hirata, A.; Kometani, T.; Miyagawa, M.; Ueda, S.-i.; Kinoshita, H.; Fujii, T.; Kuwano, M. Sensitivity to Gefitinib (Iressa, ZD1839) in Non-Small Cell Lung Cancer Cell Lines Correlates with Dependence on the Epidermal Growth Factor (EGF) Receptor/Extracellular Signal-Regulated Kinase 1/2 and EGF Receptor/Akt Pathway for Proliferation. *Mol. Cancer Ther.* **2004**, 3 (4), 465-472.